ACS APPLIED MATERIALS & INTERFACES

Research Article

www.acsami.org

Self-Healing Coatings Based on Halloysite Clay Polymer Composites for Protection of Copper Alloys

Elshad Abdullayev,*[,†,‡] Vagif Abbasov,[§] Asel Tursunbayeva,[⊥] Vasiliy Portnov,[⊥] Hikmat Ibrahimov,[§] Gulbaniz Mukhtarova,[§] and Yuri Lvov[†]

[†]Institute for Micromanufacturing, Louisiana Tech University, Ruston, Louisiana 71270, United States

[‡]Applied Minerals Inc., Dragon Mine, Silver City Rd, Eureka, Utah 84628, United States

[§]Institute of Petrochemical Processes, Azerbaijan National Academy of Sciences, Baku 1025, Azerbaijan

[⊥]Karaganda State Technical University, Karaganda 470075, Kazakhstan

Supporting Information

ABSTRACT: Halloysite clay nanotubes loaded with corrosion inhibitors benzotriazole (BTA), 2-mercaptobenzimidazole (MBI), and 2-mercaptobenzothiazole (MBT) were used as additives in self-healing composite paint coating of copper. These inhibitors form protective films on the metal surface and mitigate corrosion. Mechanisms involved in the film formation have been studied with optical and electron microscopy, UV−vis spectrometry, and adhesivity tests. Efficiency of the halloysite lumen loading ascended in the order of BTA < MBT < MBI; consequently, MBI and MBT halloysite formulations have shown the best protection. Inhibitors were kept in the tubes buried in polymeric paint layer for a long time and release was enhanced in the coating defects exposed to humid media with 20−50 h, sufficient for formation of protective layer. Anticorrosive performance of the halloysite-based composite acrylic and polyurethane coatings have been demonstrated for 110-copper alloy strips exposed to 0.5 M aqueous NaCl for 6 months.

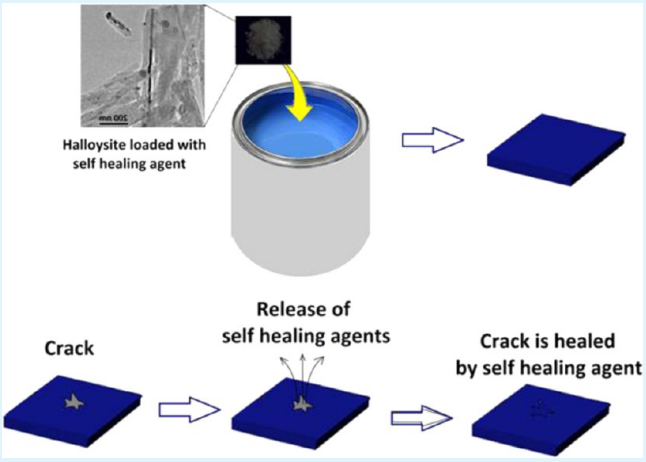

KEYWORDS: *halloysite, copper, self-healing, corrosion protection, controlled release, coatings*

INTRODUCTION

Copper alloys are widely used in electrical engineering and architecture because of their high electrical and thermal conductivity, strength, ductility, creep resistance, low thermal expansion, and solderability.[1] Corrosion is one of the most severe issues in the usage of these alloys and different coatings are used to control it. The efficiency of the usual coatings is not sufficient in aggressive environments, such as coastal areas where one could often see green corrosion spots on copper details.[2] Addition of corrosion inhibitors within protective coatings improves anticorrosive performance; however, their direct admixing into paints is not efficient because these inhibitors are easily washed away, leaving micropores in the coating.[3] Besides this, free inhibitors may react with other components of the liquid paint. Self-healing coatings containing microcapsules loaded with inhibitors and released responding to the metal corrosion is gaining a wide interest in recent years.[4−7] One of the approaches for self-repairing coatings is based on incorporation of healing agents (monomers capable of quick polymerization and anticorrosion agents) in tiny containers within paint. These agents release upon formation of defects within paint and heal the damage.[6,7] The disadvantage of this method is the requirement of high monomer content being stored in relatively large polymeric capsules of 50−100 μm diameters, which is quite challenging to be evenly dispersed within liquid paint.[4,8]

Encapsulation of corrosion inhibitors within responsive nanocontainers is an alternative promising technology for self-healing protective coatings. In this case inhibitors are released upon formation of the paint cracks and terminate metal corrosion.[4,9−11] This does not require high concentrations, as inhibitors are extremely effective even at very low concentrations and are only released in close proximity of coating defects. Nitrogen containing organics including triazoles, imidazoles, and thiazoles were studied for their copper alloy protective properties.[12−15] Three representative inhibitors: benzotriazole, 2-mercaptobenzimidazole and 2-mercaptobenzothiazole have been analyzed. Inhibition effects

Received: March 14, 2013
Accepted: April 30, 2013
Published: April 30, 2013

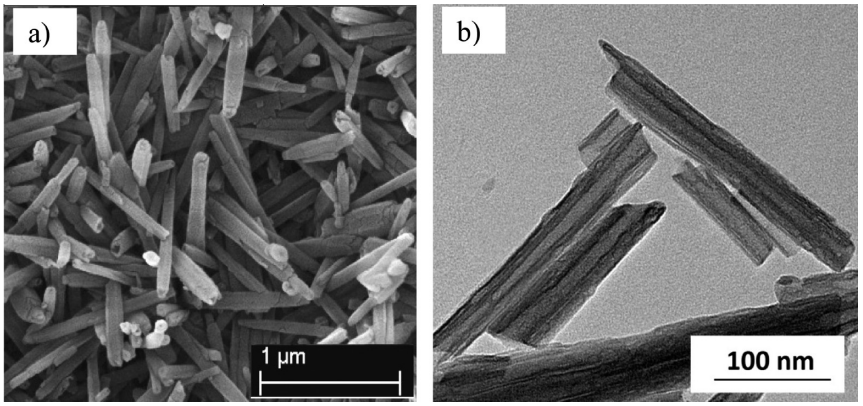

Figure 1. (a) SEM and (b) TEM images of halloysite nanotubes.

of these compounds are based on isolative film formation through interaction of metal ions and nitrogen heterocycles, while the latter two inhibitors also have thiol groups capable of additional binding on copper surface.[14]

Naturally available halloysite clay nanotubes were used for encapsulation and controlled release of a number of corrosion inhibitors.[11,16] Halloysite has empty lumen of about 15 nm diameter and ca. 1000 nm length capable for loading with chemicals. These clay tubes have been extensively studied in recent years as additives for polymer formulations and have shown remarkable improvement in the composite impact strength, adhesion, flame retardancy, and nonisothermal crystallization behavior.[17−19,21,22] Halloysite clay for self-healing coatings has been less studied, though preliminary results have been promising.[23,25] The main drawback of halloysite was the lower loading efficiency of about 5−10% by weight[24,25] (vs 40−60% in traditional polymeric microcapsules). Recently, halloysite lumen enlargement through selective alumina etching allowed for matching its loading efficiency to polymeric capsules; in addition, clay nanotubes increase strength and interlayer adhesion of the coatings.[26] Halloysite clay is easily dispersed with thermosetting resins of medium and high polarity and is an environmentally friendly material.[27−31] These attributes make halloysite a prospective candidate for self-healing anticorrosion coating formulations. In this work, polyurethane and acrylic paints doped with halloysite loaded with benzotriazole, 2-mercaptobenzimidazole, and 2-mercaptobenzothiazole corrosion inhibitors were studied for the protection of copper alloys.

MATERIALS AND METHODS

Materials. Halloysite was obtained from Applied Minerals Inc.; benzotriazole, 2-mercaprobenzimidazole, and 2-mercaptobenzothiazole were from Sigma-Aldrich. Ammonia solution was purchased from Fluka as a saturated aqueous solution (28 wt %). Sodium diethyldithiocarbamate trihydrate was received from Sigma-Aldrich as dry powder. Acrylic and polyurethane paints were purchased from Krylon and Minwax Co.

Instrumentation. Halloysite samples were characterized with a scanning electron microscope (SEM, Hitachi S 4800 FE-SEM) for external surface morphologies and the elemental composition was determined with SEM EDX analysis. Electrons were accelerated at 10−15 kV for imaging and at 25 kV for EDX elemental analysis. The samples were coated with 1.6 nm platinum by Cressington sputter coater (80 mA, 1 min) to reduce the charging effect. The internal lumen of the halloysite was analyzed with a transmission electron microscope (TEM, Zeiss EM 912) at 120 kV. Brunauer−Emmett−Teller (BET) surface analysis was performed with porosity analyzer (NOVA 2012, Quantochrome Instruments) based on nitrogen adsorption isotherms. UV−vis spectrophotometer (Agilent 8453) was used to determine the concentrations of the inhibitors and Cu (II) ions in aqueous solution. Triazole compounds concentrations were monitored at 265 nm, and copper content was measured on the absorbency peak of $[Cu(NH_3)_4]^{+2}$ complex ion at 650 nm or with sodium diethyldithiocarbamate at 450 nm (for concentration below 10 ppm). A light microscope (Olympus) with video camera (Sony SSC DC 80) was used to record corrosion spots on the metal surfaces.

Nanotube Loading. To entrap the inhibitors into halloysite nanotubes, their saturated solutions in acetone were mixed with halloysite as a dry powder. A beaker containing halloysite suspension was transferred to a vacuum jar, which was then evacuated using a vacuum pump. Slight fizzing of the suspension indicates that air is being removed from the halloysite tubes and replaced with a corrosion inhibitor. Suspension was kept under vacuum for 3 h, and then was cycled back to atmospheric pressure. This process was repeated three times to increase loading efficiency. Finally, halloysite nanotubes were separated by centrifugation, washed with water, and dried.

Corrosion Inhibitor Release Kinetics. All release experiments were performed in water, pH 6.5 at room temperature. Suspension of halloysite nanotubes was stirred with a magnetic stirrer in order to establish equilibrium conditions. Concentrations of corrosion inhibitors were determined with UV spectrophotometry. For scaling release curves, the full tube loading was determined at the end of each release experiment by finding the maximum release reached with 1 h of vigorous sonication of the samples.

Testing of Corrosion Inhibitors' Efficiency. The inhibition efficiency was tested by immersing 2.0 × 5.0 × 0.5 mm^3 size copper strips into corrosive 30 g/L NaCl aqueous solution containing 0.1 M of corrosion inhibitor.[6] Blank solution was prepared with the same composition without corrosion inhibitor. The corrosion process and inhibition efficiency were evaluated by measuring the concentration of copper ions in the media. To analyze corrosion inhibitor adsorption kinetics, we exposed three copper wafers of 7.0 × 3.3 × 0.5 mm^3 to the 30 mL of 0.25 mM solutions of benzotriazole, 2-mercaptobenzothiazole, and 2-mercaptobenzimidazole in water. Samples of solutions were collected within selected time intervals and analyzed by UV−vis spectroscopy for the inhibitor content. The same procedure was applied for the solutions of corrosion inhibitors in 0.5 M NaCl solution, simulating seawater, but the inhibitor concentration was of 1.35 mM.

Preparation and Application of Self-Healing Coating. Inhibitor loaded halloysite powder has been dispersed in water based acrylic latex paint (Krylon Corp., product no: KDH5004/KDQ5104) at 10 wt % by standard mixing with spatula. Then paint has been applied to the 1 cm × 1 cm copper strips and dried for three days. Three copper strips with 10 mm × 10 mm dimensions were coated with paint containing halloysite loaded with benzotriazole, 2-mercaptobenzimidazole, and 2-mercaptobenzothiazole and one strip with standard paint (to be used as blank). Samples were dried for 3

dx.doi.org/10.1021/am400936m | ACS Appl. Mater. Interfaces 2013, 5, 4464−4471

Scheme 1. (a) Preparation of Halloysite-Polymeric Coating, and (b) the Behaviors of the Regular and Self-Healing Coatings in Corrosion Process

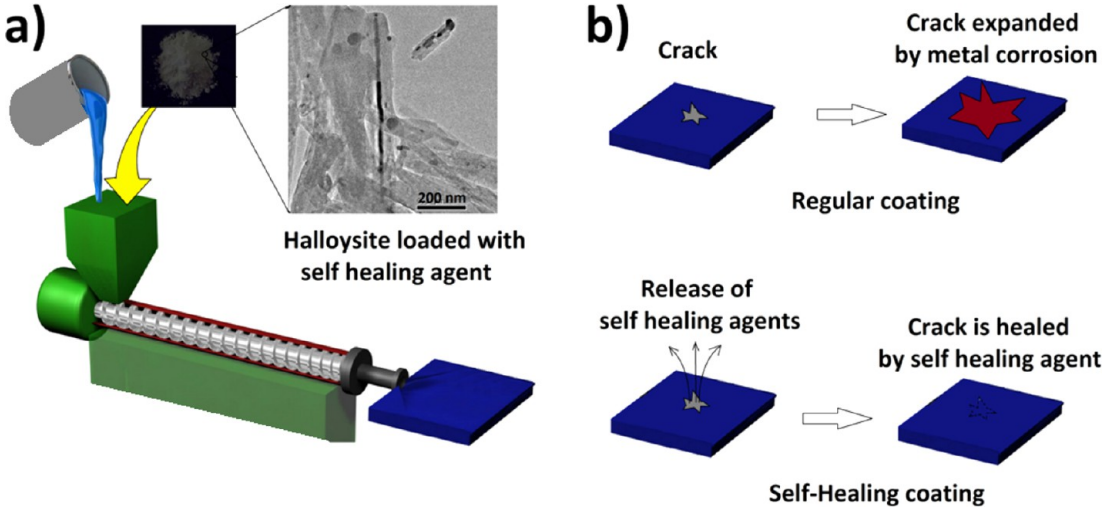

days. Backsides of the strips were coated with oil-based polyurethane paint (Minxwax Corp., Fast-Drying Polyurethane) and dried for 1 day.

Analysis of the Corrosion Spot Formation on Protective Coatings. To test anticorrosive performances, artificial 5 mm scratch has been made on all the strips with knife (acrylic paint side). Then samples were left in 30 g/L NaCl solution. The corrosion process was evaluated based on the concentration of Cu (II) ions in the environment. After 6 months strips were analyzed by light microscope for the accumulation of corrosion products at paint−metal interface. Corrosion was further evaluated by analyzing paint adhesion to copper surface using a setup similar to the balanced beam adhesion tester described in ASTM D5178 standard.

RESULTS AND DISCUSSION

Clay Nanotube Characterization. Halloysite nanotubes are formed by the rolling of alumosilicate sheets and is chemically similar to kaolinite. The single alumosilicate layer of halloysite is rolled into tube with 0.72 nm multilayer periodicity.[20,21] The outside diameter of the tubes is 60 ± 20 nm and the inner diameter is 15 ± 5 nm. The lengths of the tubes is within 500−1500 nm. Empty tubular lumens are clearly visible in the TEM image (Figure 1). Elemental composition of the used halloysite is as follows (atomic %): Al, 17.1; Si, 16.7; O, 63.3; Fe, 0.5; Ca, 1.6, which is close to theoretical ratio. Brunauer−Emmett−Teller (BET) surface area of the halloysite was 50 ± 5 m^2/g.

Self-healing coatings have been prepared by mixing mixing inhibitor loaded halloysites with the resin before applying to the metal surface (Scheme 1a). The inner lumen of halloysite makes it attractive for use as nanocontainers for encapsulating corrosion inhibitors and other active chemical agents. Encapsulation prevents unnecessary removal of the inhibitor from the coating by dissolution. Nanotubes with loaded agents stay sealed in dry paint as long as no coating cracks occur. Once the paint layer is damaged, the tube ends are exposed to the environmental moisture and loaded chemicals are released to interact with the exposed part of the metal surface to mitigate corrosion. Mechanisms involved in corrosion protection by inhibitors have been described in advanced literature.[12−15]

Selection of Corrosion Inhibitors. Benzotriazole (BTA), 2-mercaptobenzothiazole (MBT), and 2-mercaptobenzimidazole (MBI) were used as corrosion inhibitors (Scheme 2). These inhibitors form two-dimensional complexes through

Scheme 2. Chemical Structures of (a) Benzotriazole, (b) 2-Mercaptobenzothiazole, and (c) 2-Mercaptobenzimidazole

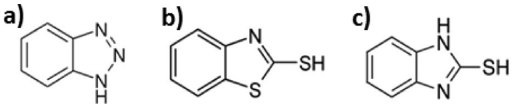

chelation with metal ions released during the corrosion process that insulate the metal surface from aggressive environment and protect from further corrosion.

The efficiency of different corrosion inhibitors were evaluated by keeping copper strips in bulk corrosive media.[13] The corrosion process was monitored by concentration of the

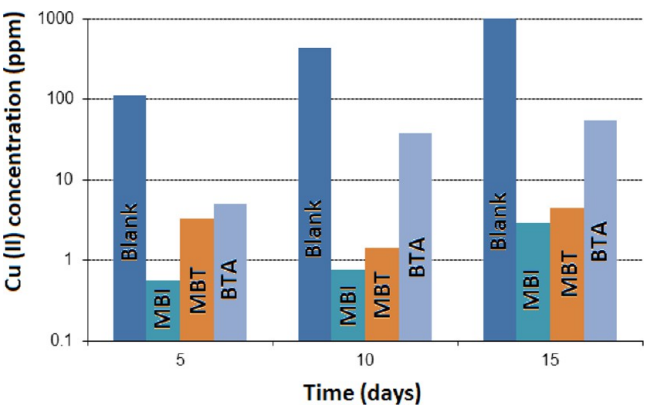

Figure 2. Copper concentration change during the corrosion test on copper strips in 30 g/L NaCl solution containing 0.1 M corrosion inhibitor (MBI, MBT, and BTA).

copper ions released to the liquid (Figure 2). Inhibition efficiency, ε, was calculated with the formula

$$\varepsilon = ([Cu^{+2}]_{blank} - [Cu^{+2}]_{inhibitor})/[Cu^{+2}]_{blank} \quad (1)$$

where $[Cu^{2+}]$ is the concentration of the copper ions released to the environment. Inhibition efficiencies after 15 days of the test were 0.950, 0.996, and 0.997 for BTA, MBT, and MBI, respectively. This data was further supported by metal weight

dx.doi.org/10.1021/am400936m | ACS Appl. Mater. Interfaces 2013, 5, 4464−4471

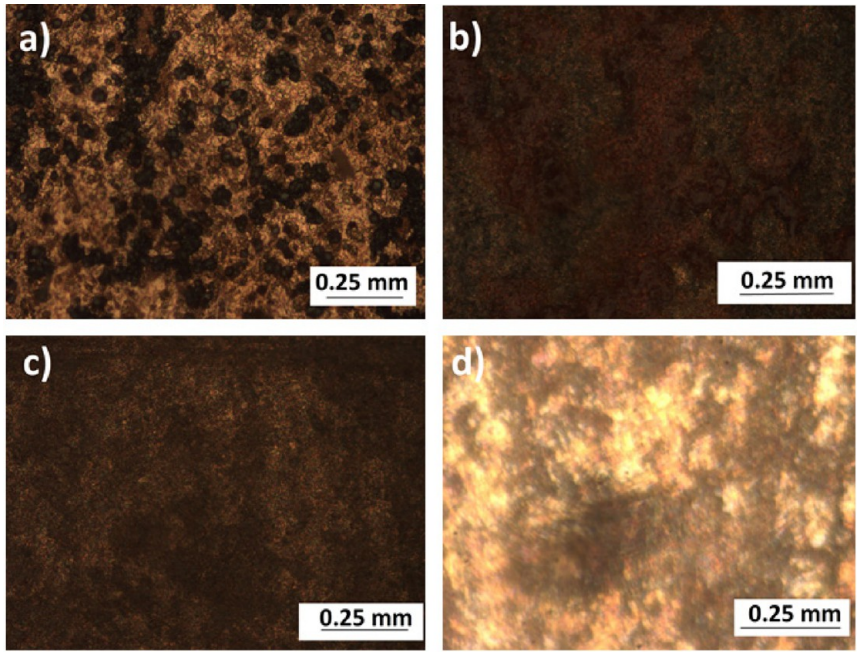

Figure 3. Optical microscope images of the copper strips after corrosion test; (a) blank, (b) BTA-, (c) MBI-, and (d) MBT-coated samples.

loss measurements. Observations of copper strips in optical microscope revealed significant amount of BTA and MBI deposition on metal strips during corrosion suppression (Figure 3). Deposition of MBT was smaller though the inhibition efficiency was superior.

Kinetics of Protective Film Formation. The corrosion inhibition is based on the formation of a thin layer of the copper-inhibitor complex that covers metal surface and insulates it.[12−15] Once the surface of the metal is completely covered with the insulating film, the reaction between the inhibitor and copper is stopped (Scheme 3a and reaction 1).

Scheme 3. Protective Layer Formation on Copper Surface in (a) Fresh and (b) Salty Water

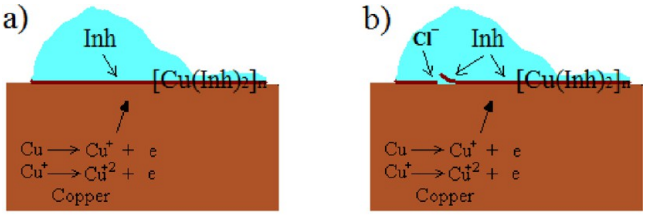

Formation of the protective film

$$1)\ Cu^{+2} + 2\,Inh \xrightarrow{k_1} [Cu(Inh)_2]_n$$

Film damage by chloride ions and rehealing

$$2)\ [Cu(Inh)_2]_n + Cl^- \xrightarrow{k_2} [CuCl(Inh)_2]^-_n + Cu$$

$$3)\ Cu^{+2} + 2\,Inh \xrightarrow{k_1} [Cu(Inh)_2]_n$$

This process follows the second order reaction kinetics, i.e., reaction rate depends on both the inhibitor concentration and the concentration of the unreacted copper atoms at the metal surface, rate = $d[Inh]/dt = k_1[Cu][Inh]$. The following equation is derived for film formation kinetics, assuming monolayer coverage of the copper surface with the inhibitor

$$a(t) = \frac{a_0 a_\infty}{a_0 - (a_0 - a_\infty)\exp(-a_\infty k_1 t/(a_0 - a_\infty))} \quad (2)$$

where, a_0, $a(t)$, and a_∞ are the initial instantaneous and final concentrations of the inhibitor, respectively (see the Supporting Information). This equation shows good fit with the experimental data (Figure 4a). Reaction rate constants derived from this model were equal to 1.3×10^{-1}, 6.5×10^{-1}, and 1.5×10^{-2} s^{-1} for BTA, MBT, and MBI, respectively. More MBT was consumed for the formation of the layer as compared to BTA and MBI, indicating higher density of the film.

For chloride containing water (like seawater), continuous consumption of the inhibitor takes place, even after complete coverage of the copper surface (Scheme 3b). This is due to the damage of the insulating films with chloride ions which demands additional supply of inhibitor for the reformation of the protective layer. Reactions 2 and 3 in Scheme 2 go in parallel. This effect has been accounted by subtracting k_2t term from the kinetic equation to obtain

$$a(t) = \frac{a_0 a_\infty}{a_0 - (a_0 - a_\infty)*\exp(-a_\infty k_1 t/(a_0 - a_\infty))} - k_2 t \quad (3)$$

which fits with experimental data fairly well (Figure 4b). Constants for the formation of the insulating films, k_1, were 0.05, 1.0, and 0.3 ± 0.03 s^{-1}, whereas reaction rate constants for the damage to the insulating layers, k_2, were 1.6×10^{-6}, 1.5×10^{-5}, and 1.2×10^{-6} mM/s for BTA, MBT, and MBI, respectively. Formation of insulating films takes place considerably faster than the film damage. Relative rate of film reformation, k_1/k_2, yields 28 100, 66 600, and 250 000 for BTA, MBT, and MBI, respectively, indicating that the inhibitor response to the damaged film descents in the order of MBI > MBT > BTA. The kinetics also correlate with the corrosion inhibition efficiencies described previously.

One can clearly observe that significantly more MBT was consumed for the monolayer film formation as compared to BTA and MBI. This result seems to be in contradiction with

dx.doi.org/10.1021/am400936m | ACS Appl. Mater. Interfaces 2013, 5, 4464−4471

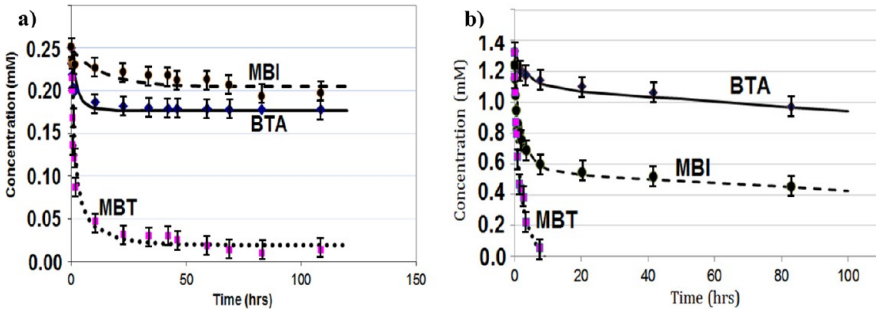

Figure 4. Adsorption of BTA, MBI, and MBT on copper surface in (a) fresh and (b) salty 30 g/L NaCl water.

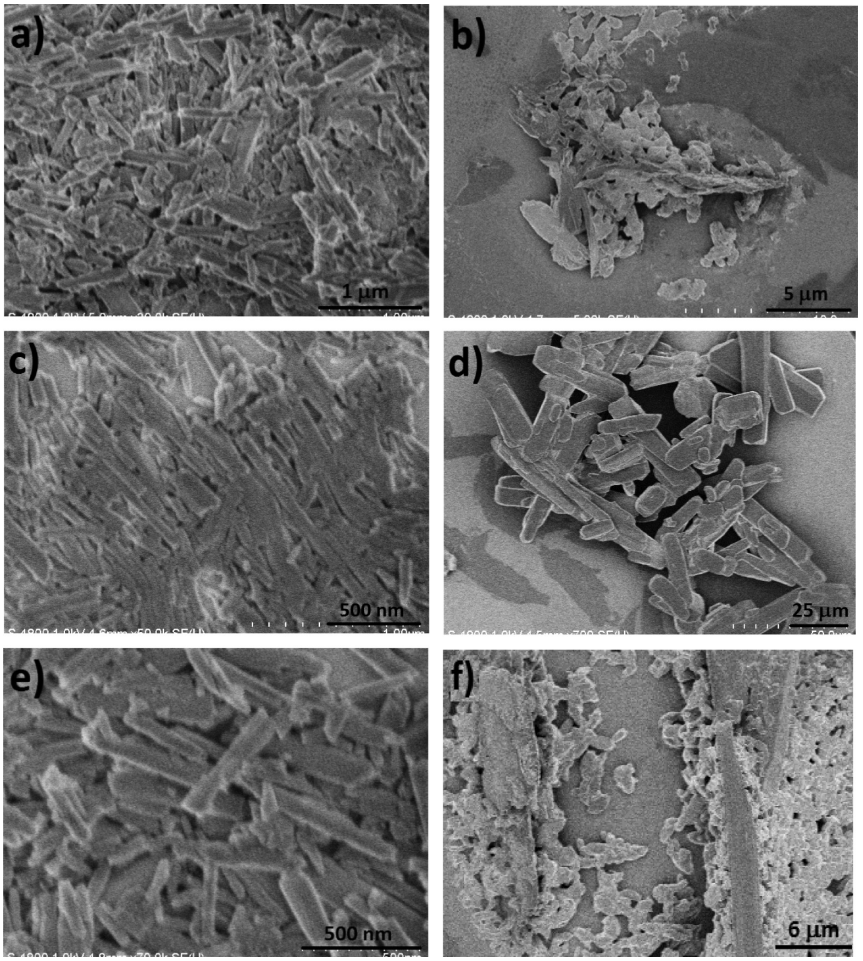

Figure 5. SEM images of halloysite nanotubes loaded with (a) BTA, (c) MBI, and (e) MBT (left); and microcrystals of the inhibitors (b) BTA, (d) MBI, and (f) MBT (right).

the analysis on film formation by optical microscope (Figure 3). However, one should note the difference in the concentrations of the inhibitors used. Significantly higher concentration of inhibitors (100 mM) was used for testing inhibition efficiencies compared to the kinetic study (1.3 mM). Such a high concentration results in multilayer coverage of the copper surface with protective film in the case of BTA and MBI (vs monolayer coverage in kinetics study). Multilayer coverage was effectively suppressed in the case of MBT, which is believed to be associated with the higher density of the monolayer film. Indeed, two sulfur atoms in MBT are expected to coordinate with surface copper atoms more effectively compared to the other inhibitors.

Encapsulation of Inhibitors within Clay Nanotubes. Vacuum cycling has been used to load halloysite with corrosion inhibitors. Acetone was the optimal solvent for loading active agents because of (a) their higher solubility in acetone (b) the lower viscosity of acetone compared to water, giving faster diffusion into tubes, and c) the evaporation of acetone is faster under vacuum, resulting in higher concentration gradient during loading process. SEM images of the halloysites loaded with corrosion inhibitors (washed and dried) are presented in Figure 5. No crystals of free inhibitors have been observed, indicating that all the substances have been loaded within tube lumen. Original inhibitors form much larger microcrystals than the halloysite lumen size. The loaded inhibitors are in

amorphous state, which is supported by X-ray data containing no crystal reflections additional to the halloysite diffraction patterns (see the Supporting Information, XRD data, Figure S1).

Release of Corrosion Inhibitors. Loaded corrosion inhibitors released from the nanotubes and, for comparison, release from free microcrystals also analyzed (Figure 6). Release

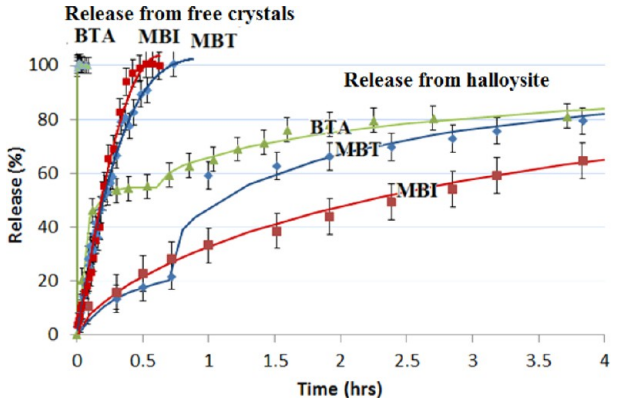

Figure 6. Release profiles of corrosion inhibitors: BTA, MBI, and MBT from free crystals and from halloysite tubes in DI water with magnetic stirring.

from halloysite tubes is considerably slower and extends over 20−30 h. 99% release of MBI was achieved within 35 h, which is 50-times slower than the release from its microcrystals. BTA and MBT release from halloysite takes place in two stages, while MBI release occurs in single stage. Initial fast release of BTA and MBT is associated with dissolution of externally adsorbed inhibitors. Two stage release profile was also reported for tetracycline hydrochloride−halloysite.[32] External adsorption of corrosion inhibitors is undesirable because it releases much faster than nanopore diffusion controlled regime from the tube lumen. Closer inspection of the release curves indicate that the lumen loading increases in the order of BTA < MBT < MBI. All the MBI is loaded within the halloysite lumen, whereas about half of the BTA is adsorbed outside. Absolute loading efficiencies of the inhibitors were about 4.0, 19.0, and 25.0% for BTA, MBT, and MBI, respectively.

Corrosion Tests with Halloysite/Polymer Composite Coating. Corrosion tests were performed on 110 copper alloy strips; four strips were coated with transparent polyurethane paint on one side and acrylic latex paint on the other side. One strip was coated with pure acrylic and polyurethane paints (blank), whereas three others were coated with the paint composites containing 10 wt % halloysite loaded with the inhibitors. After complete curing for 3 days, coatings were artificially scratched and exposed to salt water containing 0.5 M of NaCl for 6 months. Corrosion process was monitored by measuring the concentration of the Cu(II) ions released (Figure 7a). Extensive release of metal ions from blank sample indicates severe corrosion process taking place on the metal. Green patina observed underneath the paint also indicates severe corrosion (Figure 7b). Adding halloysite loaded with corrosion inhibitors significantly reduced corrosion in all the composite coatings. Some corrosion was developed within the first fifteen days, which is evident from the rise of the Cu (II) ions in the solution, but then it was suppressed with the release of inhibitors in the coating defects. The black corrosion spot

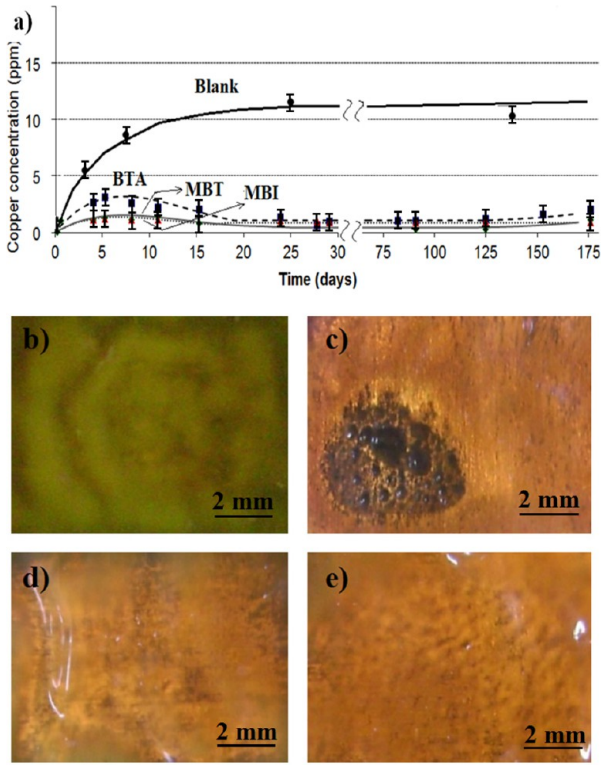

Figure 7. (a) Copper concentration in the corrosive environment for copper strips coated with halloysite paint composite and optical images of the strips through transparent polyurethane film; (b) blank coating, and protective halloysite coating loaded with (c) BTA, (d) MBI, and (e) MBT.

observed for BTA loaded halloysite paint (Figure 7c) is due to this initial corrosion process.

Composite Coating Adhesion. The adhesion test is an alternative measure of the undercoat corrosion. Poor adhesion of the coating at metals is indication of severe damage due to accumulation of corrosion products at the interface. A setup similar to the beam adhesion tester described in ASTM D5178 standard method has been used (Scheme 4). A load was applied

Scheme 4. Setup for Testing Paint Adhesion to the Metal

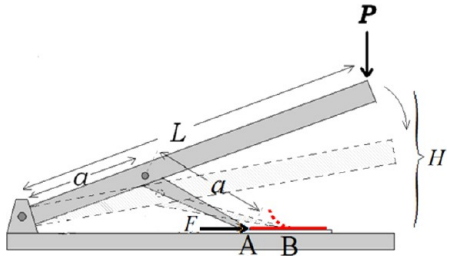

to the end of the beam (P) with tensile tester causing the arm to move from point A to B and detach the coating from the metal surface. The peeling force (F) exerted by metal arm to the paint is obtained with simple geometric considerations

$$F = (PL)/(a\mathrm{tg}(\beta)) \quad (3)$$

where a and L are the dimensions of the apparatus and $\mathrm{tg}(\beta)$ is the tangent of the beam inclination angle $\beta = \sin^{-1}\{H/L\}$, H is the height of the beam.

dx.doi.org/10.1021/am400936m | ACS Appl. Mater. Interfaces 2013, 5, 4464−4471

The original paint has strong adhesion to the metal surface, yielding a maximum peeling force of 63 N. On the other hand, corroded paint does not show distinct force maxima and paint started peeling off at 9 N, indicating that the entire paint is loosely attached to the metal surface contaminated with corrosion products. All the halloysite-based composite coatings analyzed after corrosive exposure had maximum peeling force of 41 ± 2 N before cracking, which is very good in comparison with usual paint coating. It is less than the original coating adhesion before the corrosion indicating that some corrosion has taken place (Table 1). In separate study, we found a drastic increase (2−3 times) on interlayer adhesivity for paint coatings doped with halloysite, which is most likely related to partial clay tube interpenetration between the paint layers.

Table 1. Composite Coating Adhesive Forces on Strips of 110-Copper Alloy after 6 Months of Exposure to the 30 g/L NaCl Solution

coating type	max peeling force (N)
blank polyurethane paint, before corrosion	63 ± 5
blank polyurethane paint, after corrosion	9 ± 1
paint with halloysite-BTA, after corrosion	40 ± 2
paint with halloysite-MBT, after corrosion	42 ± 2

CONCLUSIONS

Natural halloysite clay nanotubes were employed as inexpensive nanocontainers for the entrapment of corrosion inhibitors into metal polymer coatings to provide sustained release. Inhibitive actions of three inhibitors; benzotriazole, 2-mercaptobenzimidazole, and 2-mercaptobenzothiazole have been studied on metallic copper strips. Benzotriazole and 2-mercaptobenzimidazole formed visible isolative multilayer films on metal surface, whereas 2-mercaptobenzothiazole formed thinner films. Isolative coating damage occurs in chloride solution (such as seawater) that requires sustained supply of inhibitors to heal corrosion defects, which were delivered in our technique with slow release from clay nanotubes in defect areas. A rate of healing efficiency, defined as the ratio of protective film formation rate vs chlorine film damage vary at 28 000−250 000 for these inhibitors, indicating effective chloride pit healing. Halloysites loaded with these inhibitors at 5−20 wt % were utilized as additives for anticorrosive coatings. Inhibitors were successfully loaded within halloysite tubes, with 2-mercaptobenzimidazole being the most efficient in the loading capacity. Inhibitor-loaded halloysites significantly improved anticorrosive performance of the polyurethane and acrylic coatings applied on copper strips tested for 6 months in 0.5 M NaCl solution simulating seawater. Corrosion was retarded at the initial stage because of the inhibitive action of the inhibitors leaking from halloysite in the coating cracks. Paint adhesion to the copper surface was five times higher in the case of halloysite-based composite coating after the corrosion test.

ASSOCIATED CONTENT

Supporting Information

Derivation of the kinetic equation for inhibitor film formation; X-ray powder diffraction patterns (Cu−Kα radiation) of the empty pristine halloysite and halloysite loaded with BTA, MBT, and MBI; optical microscope images of copper surface underneath the coating after 6 months of corrosion test; paint with halloysite loaded with (a) BTA-benzotriazole, (b) 2-mercaptobenzimidazole, and (c) 2-mercaptobenzothiazole. This material is available free of charge via the Internet at http://pubs.acs.org.

AUTHOR INFORMATION

Corresponding Author

*E-mail: eabdullayev@appliedminerals.com.

Notes

The authors declare no competing financial interest.

ACKNOWLEDGMENTS

We are grateful to Andre Zeitoun (Applied Minerals, Inc.) for providing halloysite samples. Support by NSF CMMI-102914, EPS-1003897 grants and Louisiana Board of Regents ITRS grants are acknowledged. Any opinions, findings, and conclusions or recommendations expressed in this report are those of authors and do not necessarily reflect the view of National Science Foundation.

REFERENCES

(1) Davis, J. R. *ASM Specialty Handbook: Copper and Copper Alloys*; ASM International: Materials Park, OH, 2001.
(2) Schweitzer, P. A. *Corrosion of Linings and Coatings: Cathodic and Inhibitor Protection and Corrosion Monitoring*; CRC Press, Taylor & Francis Group: Boca Raton, FL, 2007.
(3) Palanivela, V.; Huangb, Y.; Van Ooija, W. J. *Progr. Org. Coat.* **2005**, *53*, 153−168.
(4) Shchukin, D.; Möhwald, H. *Small* **2007**, *3*, 926−943.
(5) Abdullayev, E.; Price, R.; Shchukin, D.; Lvov, Y. *ACS Appl. Mater. Interfaces* **2009**, *1*, 1437−1443.
(6) Sottos, N.; White, S.; Bond, I. *J. Roy. Soc. Interfaces* **2007**, *4*, 347−348.
(7) White, S.; Sottos, N.; Geubelle, P.; Moore, J.; Kessler, M.; Sriram, S.; Brown, E.; Viswanathan, S. *Nature* **2001**, *409*, 794−797.
(8) Blaiszik, B.; Sottos, N.; White, S. *Compos. Sci. Technol.* **2008**, *68*, 978−986.
(9) Abdullayev, E.; Lvov, Y. *J. Mater. Chem.* **2010**, *20*, 6681−6687.
(10) Shchukin, D.; Möhwald, H. *Adv. Funct. Mater.* **2007**, *17*, 1451−1458.
(11) Abdullayev, E.; Lvov, Y. *J. Nanosci. Nanotechnol.* **2011**, *11*, 10007−10026.
(12) Sease, C. *Stud. Conserv.* **1978**, *23*, 76−85.
(13) Faltermeier, R. *Stud. Conserv.* **1998**, *44*, 121−128.
(14) Antonijevic, M.; Petrovic, M. *Int. J. Electrochem. Sci.* **2008**, *3*, 1−28.
(15) Otmacic, H.; Lisac, E. *Electrochim. Acta* **2003**, *48*, 985−991.
(16) Joshi, A.; Abdullayev, E.; Vasiliev, A.; Volkova, O.; Lvov, Y. *Langmuir* **2013**, DOI: 10.1021/la3044973.
(17) Shi, X.; Nguyen, T.; Suo, Z.; Liu, Y.; Avci, R. *Surf. Coat. Technol.* **2009**, *204*, 237−245.
(18) Ye, Y.; Chen, H.; Wu, J.; Ye, L. *Polymer* **2007**, *48*, 6426−6433.
(19) Du, M.; Guo, B.; Jia, D. *Polym. Int.* **2010**, *59*, 574−582.
(20) Abdullayev, E.; Sakakibara, K.; Okamoto, K.; Wei, W.; Ariga, K.; Lvov, Y. *ACS Appl. Mater. Interfaces* **2011**, *3*, 4040−4046.
(21) Wei, W.; Abdullayev, E.; Hollister, A.; Lvov, Y.; Mills, D. *Macromol. Mater. Eng.* **2012**, *301*, 645−653.
(22) Guo, B.; Zou, Q.; Lei, Y.; Du, M.; Liu, M.; Jia, D. *Thermochim. Acta* **2009**, *484*, 48−56.
(23) Fix, D.; Andreeva, D.; Shchukin, D.; Lvov, Y.; Möhwald, H. *Adv. Funct. Mater.* **2009**, *19*, 1720−1727.
(24) Abdullayev, E.; Shchukin, D.; Lvov, Y. *Polym. Mater.: Sci. Eng.* **2008**, *99*, 331−332.
(25) Shchukin, D.; Lamaka, S.; Yasakau, K.; Zheludkevich, M.; Fereira, M.; Möhwald, H. *J. Phys. Chem. C* **2008**, *112*, 958−964.
(26) Abdullayev, E.; Joshi, A.; Wei, W.; Zhao, Y.; Lvov, Y. *ACS Nano* **2012**, *6*, 7216−7226.

(27) Skiba, M.; Kulok, M.; Kołacz, R.; Skiba, T., , *Proceedings of the 19th European Symposium on Quality of Poultry Meat and 13th European Symposium on the Quality of Eggs and Egg Products*; Turku, Finland, June 21−25, 2009 ; World Poultry Science Association: Beekbergen, The Netherlands, 2009; pp 1−9.
(28) Liu, M.; Guo, B.; Du, M.; Yanda Lei, Y.; Jia, D. *J. Polym. Res.* **2008**, *15*, 205−212.
(29) Li, X.; Nikiforow, I.; Pohl, K.; Adams, J.; Johannsmann, D. *Coatings* **2013**, *3*, 16−25.
(30) Vergaro, V.; Abdullayev, E.; Lvov, Y. M.; Cingolani, R.; Rinaldi, R.; Leporatti, S. *Biomacromolecules* **2010**, *11*, 820−828.
(31) Kommireddy, D. S.; Ichinose, I.; Lvov, Y. M.; Mills, D. K. *J. Biomed. Nanotechnol.* **2005**, *1*, 286−290.
(32) Ward, C.; Song, S.; Davis, E. *J. Nanosci. Nanotechol.* **2010**, *10*, 6641−6649.